Observation of Quantum-Limited Spin Transport in Strongly Interacting Two-Dimensional Fermi Gases

C. Luciuk,[1] S. Smale,[1] F. Böttcher,[2] H. Sharum,[1] B. A. Olsen,[1] S. Trotzky,[1] T. Enss,[3] and J. H. Thywissen[1,4]
[1]Department of Physics, University of Toronto, Ontario M5S 1A7, Canada
[2]5. Physikalisches Institut and Centre for Integrated Quantum Science and Technology, Universität Stuttgart, D-70569 Stuttgart, Germany
[3]Institut für Theoretische Physik, Universität Heidelberg, D-69120 Heidelberg, Germany
[4]Canadian Institute for Advanced Research, Toronto, Ontario M5G 1Z8, Canada
(Received 20 December 2016; published 31 March 2017)

We measure the transport properties of two-dimensional ultracold Fermi gases during transverse demagnetization in a magnetic field gradient. Using a phase-coherent spin-echo sequence, we are able to distinguish bare spin diffusion from the Leggett-Rice effect, in which demagnetization is slowed by the precession of a spin current around the local magnetization. When the two-dimensional scattering length is tuned to be comparable to the inverse Fermi wave vector k_F^{-1}, we find that the bare transverse spin diffusivity reaches a minimum of $1.7(6)\hbar/m$, where m is the bare particle mass. The rate of demagnetization is also reflected in the growth rate of the s-wave contact, observed using time-resolved spectroscopy. The contact rises to $0.28(3)k_F^2$ per particle, which quantifies how scaling symmetry is broken by near-resonant interactions, unlike in unitary three-dimensional systems. Our observations support the conjecture that, in systems with strong scattering, the local relaxation rate is bounded from above by $k_BT/\hbar$.

DOI: 10.1103/PhysRevLett.118.130405

Conjectured quantum bounds on transport appear to be respected and nearly saturated by quark-gluon plasmas [1,2], unitary Fermi gases [3–11], and bad metals [12,13]. For many modalities of transport, these bounds can be recast as an upper bound on the rate of local relaxation to equilibrium $1/\tau_r \lesssim k_BT/\hbar$, where k_B is the Boltzmann constant and T is the temperature [14,15]. Systems that saturate this "Planckian" bound do not have well-defined quasiparticles promoting transport [1,12–15]. A canonical example is the quantum critical regime, where one expects diffusivity $D \sim \hbar/m$, a ratio of shear viscosity to entropy density $\eta/s \sim \hbar/k_B$, and a conductivity that is linear in T [4,12,13]. These limiting behaviors can be understood by combining τ_r with a propagation speed $v \sim \sqrt{k_BT/m}$, for example, $D \sim v^2\tau_r$. This argument applies to ultracold three-dimensional (3D) Fermi gases, whose behavior in the strongly interacting regime is controlled by the quantum critical point at a divergent scattering length, zero temperature, and zero density [4,16,17]. In such systems, one observes $D \gtrsim 2\hbar/m$ [6–8] and $\eta/s \gtrsim 0.4\hbar/k_B$ [3], compatible with conjectured quantum bounds.

However, in attractive two-dimensional (2D) Fermi gases, scale invariance is broken by the finite bound-state pair size, so the strongly interacting regime is no longer controlled by a quantum critical point [16,18–23]. Strikingly, an extreme violation of the conjectured $D \gtrsim \hbar/m$ bound has been observed in the spin dynamics of an ultracold 2D Fermi gas: an apparent diffusivity of $6.3(8) \times 10^{-3}\hbar/m$ near $\ln(k_Fa_{2D}) = 0$ [24], where k_F is the Fermi momentum and a_{2D} is the 2D s-wave scattering length. No similarly dramatic effect of dimensionality is observed in charge conductivity [12] or bulk viscosity [25], and such a low spin diffusivity is unexplained by theory [11,19].

In this work, we recreate the conditions of Ref. [24] and study the demagnetization dynamics of ultracold 2D Fermi gases using both a coherent spin-echo sequence [8] and time-resolved spectroscopy [7]. We find a modification of the apparent diffusivity by the Leggett-Rice (LR) effect [26]; however, in disagreement with Ref. [24], we find that the quantum bound for the spin diffusivity is satisfied in all conditions accessible to our apparatus. Near $\ln(k_Fa_{2D}) = 0$, where the minimum diffusivity is observed, we quantify the breaking of scale invariance by measuring the contact, whose magnitude suggests that the gas is in a many-body excited state during demagnetization.

Our experiments use the three lowest-energy internal states, labeled $|-z\rangle$, $|+z\rangle$, and $|\mathrm{pr}\rangle$, of neutral ^{40}K atoms. Interactions between $|-z\rangle$ and $|+z\rangle$ atoms are tuned by the s-wave Feshbach resonance [27] at 202.1 G, while $|\mathrm{pr}\rangle$ atoms remain weakly interacting with $|\pm z\rangle$ atoms, and any atoms in identical spin states are noninteracting, since the gas is ultracold. An ensemble of 2D systems is prepared by loading a sympathetically cooled 3D cloud of $|-z\rangle$ atoms into an optical lattice with a period of 380 nm along the x_3 direction [28]. At the final lattice depth of $V_0 = 50E_R$, where $E_R/\hbar \simeq 2\pi \times 8.64$ kHz, the 2D samples are isolated from one another and in near-harmonic confinement with $\omega_3 \simeq 2\pi \times 122$ kHz. The transverse confinement with $\omega_{1,2} \simeq 2\pi \times 600$ Hz is controlled by an optical dipole trap. Immediately after loading, the 2D clouds are not rigorously

in thermal equilibrium, but thermalization within each plane occurs once demagnetization commences. The effective initial temperature $(T/T_F)_i$ (assigned assuming isentropic loading of the lattice [28]) can be varied between 0.20 and 1.20, where $T_F \equiv E_F/k_B$ and $E_{Fi} = \hbar^2 k_{Fi}^2/2m$ is the Fermi energy of the central 2D system in its initial polarized state. A static magnetic field gradient B' along x_1 is set to 20.3(2) G/cm unless stated otherwise.

Transport of local magnetization $\boldsymbol{M} = \langle M_x, M_y, M_z \rangle$ occurs through a spin current $\boldsymbol{J}_j$ that can be decomposed into a longitudinal component ($\boldsymbol{J}_j^{\parallel} \| \boldsymbol{M}$) and a transverse component ($\boldsymbol{J}_j^{\perp} \perp \boldsymbol{M}$), where bold letters indicate vectors in Bloch space and the subscript $j \in \{1, 2, 3\}$ denotes spatial direction. Our measurements follow a standard spin-echo protocol [29] that initiates a purely transverse current. In the hydrodynamic regime, $\boldsymbol{J}_j^{\perp}$ is the sum of a dissipative term $-D_{\text{eff}}^{\perp} \nabla_j \boldsymbol{M}$ and a reactive term $-\gamma \boldsymbol{M} \times D_{\text{eff}}^{\perp} \nabla_j \boldsymbol{M}$, where $D_{\text{eff}}^{\perp} = D_0^{\perp}/(1 + \gamma^2 M^2)$ is the effective transverse diffusivity and $D_0^{\perp}$ is the bare diffusivity [26]. The parameter γ quantifies the precession of the spin current about the local magnetization, which slows demagnetization—a phenomenon known as the Leggett-Rice effect.

Dynamics are initiated by a resonant radio-frequency (rf) pulse with area θ, which creates a superposition of $|-z\rangle$ and $|+z\rangle$ and thus a magnetization $M_z = -\cos(\theta)$ and $M_{xy} \equiv M_x + iM_y = i\sin(\theta)$. The field gradient causes a twisting of the xy magnetization into a spiral texture. The gradient in the direction of $\boldsymbol{M}$ drives a transverse spin current $\boldsymbol{J}_1^{\perp}$, which tends to relax $M_{xy} \to 0$, while M_z is conserved. These dynamics are described by [26]

$$\partial_t M_{xy} = -i\alpha x_1 M_{xy} + D_{\text{eff}}^{\perp}(1 + i\gamma M_z)\nabla_1^2 M_{xy}, \quad (1)$$

where $\alpha = B'\Delta\mu/\hbar$ and $\Delta\mu$ is the difference in the magnetic moment between $|+z\rangle$ and $|-z\rangle$. The solutions of Eq. (1) depend on a dimensionless time $R_M t_h$, where t_h is the total hold time between the initialization pulse and final readout pulse and $R_M \equiv (D_0^{\perp}\alpha^2)^{1/3}$ [28]. In our typical conditions, R_M^{-1} is on the order of 1 ms.

We measure the vector magnetization using a spin-echo sequence as shown in Fig. 1(a). A π pulse at time $t_h/2$ reverses all M_{xy} phases, so that evolution in the presence of B' causes an untwisting of the spiral magnetization texture. The final $\pi/2$ pulse is applied with a variable phase lag relative to the initialization pulse. The contrast in the final populations in $|\pm z\rangle$ is used to determine the direction $\phi = \arg(M_{xy}/i)$ and the magnitude $|M_{xy}|$ of the transverse magnetization.

Figures 1(b) and 1(c) show an example of $|M_{xy}(t_h)|$ and $\phi(t_h)$, for an initial pulse angle $\theta = 0.25\pi$. The solution of Eq. (1) for $\gamma \neq 0$ gives $\phi = \gamma M_z \ln|M_{xy}/M_{xy}(0)|$ for all t_h, and thus γ is found by linear regression on data such as Fig. 1(c). Then, R_M (and from it $D_0^{\perp}$) is determined by a nonlinear fit to $|M_{xy}(t_h)|$ data, again using an analytic solution of Eq. (1). $M_{xy}(0)$ and B' are independently calibrated [28].

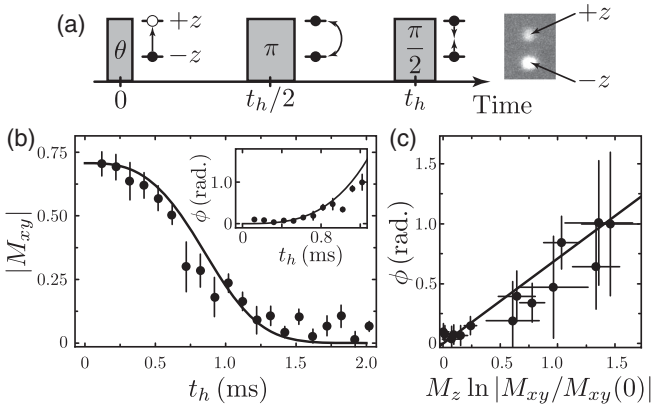

FIG. 1. Magnetization dynamics. (a) The time sequence used to measure the magnetization dynamics is a simple spin-echo sequence which allows us to measure (b) the amplitude and phase (inset) of the ensemble-averaged transverse magnetization. Populations are measured with absorption imaging after a Stern-Gerlach separation [28]. Data are shown for $\theta = 0.25\pi$, which prepares $M_z = -0.71$. (c) γ is found from the slope of $\phi(t_h)$ versus $M_z \ln|M_{xy}/M_{xy}(0)|$.

For the data shown in Fig. 1, at $\ln(k_{Fi}a_{2D}) = 0.13(3)$ and $(T/T_F)_i = 0.36(4)$, we find $D_0^{\perp} = 2.3(3)\hbar/m$ and $\gamma = 0.6(1)$. These best-fit transport coefficients are understood as an average both over the ensemble of 2D systems and over the dynamical changes in the cloud, discussed below. For strong interactions when the mean free path ~ 1 μm is much smaller than the Thomas-Fermi length and the typical minimal spin-helix pitch ~ 5 μm, we expect that the trap-averaged transport coefficients are close to the homogeneous values. In this regime, the dynamics are essentially local [30].

We search for conditions that minimize $D_0^{\perp}$ by repeating this characterization of $M_{xy}(t_h)$ at various interaction strengths and initial temperatures. Figure 2(a) shows that $D_0^{\perp}$ is smallest when $-0.5 \lesssim \ln(k_{Fi}a_{2D}) \lesssim +0.5$, i.e., where a_{2D} is comparable to k_F^{-1}. This condition can be understood by considering the 2D scattering amplitude in vacuum: $f(k) = 2\pi/[-\ln(ka_{2D}) + i\pi/2]$ [23,31–33], which gives a maximal (unitary) cross section $4/k$ at $ka_{2D} = 1$. Even though our Fermi gas has a distribution of relative momenta k, the average cross section at a low temperature can be estimated by the replacement of k with k_F, due to the logarithmic dependence of f on the energy of the collision. In other words, corrections to the unitary scattering cross section are only logarithmic [18–22,34], which explains the qualitative similarity of Fig. 2(a) to prior 3D measurements [8].

The lines in Fig. 2(a) show a kinetic theory both with and without medium scattering (solid and dashed lines, respectively) calculated in the $|\boldsymbol{M}| \to 1$ limit [11,30]. The model also accounts for inhomogeneities in the following way.

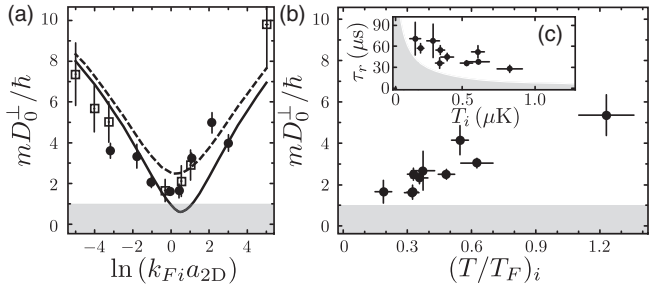

FIG. 2. Transverse spin diffusivity. (a) $D_0^\perp$ versus interaction strength $\ln(k_{Fi}a_{2D})$ with $(T/T_F)_i = 0.31(2)$ (black circles) and $(T/T_F)_i = 0.21(3)$ (open squares). Each data point corresponds to a complete data set as shown in Fig. 1. The lines are predictions for $T/T_F = 0.3$ by a kinetic theory, as described in the text. (b) $D_0^\perp$ versus the initial reduced temperature $(T/T_F)_i$ at $\ln(k_{Fi}a_{2D}) = -0.1(2)$. (c) Local relaxation rate τ_r estimated as $D_0^\perp/v_T^2$. Shaded regions show $D_0^\perp < \hbar/m$ in (a),(b) and $\tau_r < \hbar/k_BT$ in (c). Data are consistent with the conjectured quantum bound, which would exclude the shaded areas on all plots.

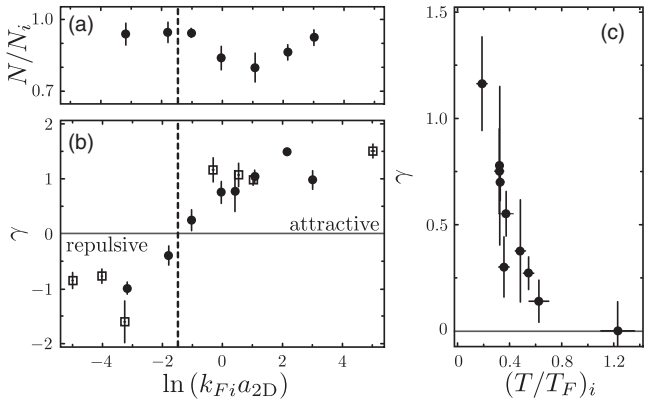

FIG. 3. Change in the sign of the interaction. (a) The fraction of atoms remaining at $t_h = 3.5$ ms. (b) γ vs the interaction strength, with $(T/T_F)_i = 0.31(2)$ (black circles) and $(T/T_F)_i = 0.21(3)$ (open squares). (c) γ versus the initial reduced temperature $(T/T_F)_i$, at $\ln(k_{Fi}a_{2D}) = -0.1(2)$. The change in the sign of γ, at $\ln(k_{Fi}a_{2D}) \approx -1$, is associated with the onset of a pairing instability.

First, the collision integral is solved to compute the transverse spin diffusion time and LR parameter for a 2D homogeneous system with the same spin density and temperature as the trap center [11,35]. Next, these parameters are used to solve the Boltzmann equation for the position-dependent spin density in the full trapping potential for each 2D gas in the ensemble [30]. Finally, the average magnetization dynamics is analyzed using Eq. (1). This procedure predicts a minimal $D_0^\perp$ slightly shifted from the observed minimum, but its results agree well with the increase of $D_0^\perp$ in the weakly interacting regime. This gives us confidence that inhomogeneity effects are well understood.

The lowest observed diffusivity is $D_0^\perp = 1.7(6)\hbar/m$, at $(T/T_F)_i = 0.19(3)$ and $\ln(k_{Fi}a_{2D}) = -0.1(2)$. The effect of the temperature is shown in Fig. 2(b) and by data sets in Fig. 2(a) taken at two temperatures. In all cases, our data support the conjectured bound $D_0^\perp \gtrsim \hbar/m$.

Assuming that magnetization perturbations propagate at $v_T \sim \sqrt{k_BT/m}$, one can estimate the local relaxation time τ_r with $D_0^\perp/v_T^2$. Figure 2(c) compares this time to the bound $\hbar/k_BT$. Another estimate of the relaxation time would use the Fermi velocity v_F, as $\tau_r \sim 2D_0^\perp/v_F^2$, which is the correct scaling for the mean free time in imbalanced Fermi liquids at a low temperature [26,28,35]. This yields $\tau_r \sim 20$ μs at the minimum observed diffusivity, again on the order of $\hbar/k_BT$. In sum, a 2D Fermi gas with $a_{2D}k_F \sim 1$ seems to saturate, but not violate, the Planckian bound $\tau_r^{-1} \lesssim k_BT/\hbar$ at the lowest temperatures probed here.

Figures 3(b) and 3(c) summarize measurements of γ across a wide range of interaction strengths and temperatures. There are two implications of these data. First, system-wide demagnetization is slowed by the spin current precession. At short t_h, the solution to Eq. (1) is $|M_{xy}|/|M_{xy}(0)| = \exp(-D_{\rm eff}^\perp \alpha^2 t_h^3/12)$, with an apparent diffusivity $D_{\rm eff}^\perp$, which is $= D_0^\perp/(1+\gamma^2)$ for a fully polarized cloud. This functional form was used in Ref. [24] to determine a minimum "$D_s^\perp$" of $6.3(8)\times 10^{-3}\hbar/m$. In similar conditions, we instead find $D_{\rm eff}^\perp = 7(3)\times 10^{-1}\hbar/m$. In both works, diffusivity is observed to be minimal near $\ln(k_{Fi}a_{2D}) = 0$ and to double between $\ln(k_{Fi}a_{2D}) \approx 0$ and $\ln(k_{Fi}a_{2D}) \approx 1$. However, we cannot explain the 100-fold difference in scale.

The second implication of γ is to reveal the sign of the interaction between the spin current and the local magnetization [26,36,37]. When $\gamma < 0$, as we observe for $\ln(k_{Fi}a_{2D}) \lesssim -1.5$ [see Fig. 3(b)], interactions are repulsive, whereas when $\gamma > 0$, as we observe for $\ln(k_{Fi}a_{2D}) \gtrsim -1.5$, interactions are attractive. Associated with the sign change of γ is the onset of a pairing instability, since both are related to the sign change of the real part of the low-energy scattering $\mathcal{T}$ matrix [8,11,38]. We find indirect evidence for this from atom loss [see Fig. 3(a)], since Feshbach dimers are a precursor to the formation of deeply bound molecules [39], which are lost from the trap. In 3D, this loss rate is higher on the repulsive side of unitarity, but in 2D, we observe the strongest loss on the attractive side, at $\ln(k_{Fi}a_{2D}) \sim 1$ [40]. We discuss this further below.

One consequence of demagnetization is a cloud-wide redistribution of energy. For a 2D harmonically trapped Fermi gas, the virial relation is [41]

$$V = \frac{1}{2}E + \frac{\hbar^2}{8\pi m}\mathcal{C}_{2D}, \tag{2}$$

where V is the total potential energy, E is the total energy, and $\mathcal{C}_{2D}$ is the (extensive) 2D contact [41,42]. Even though

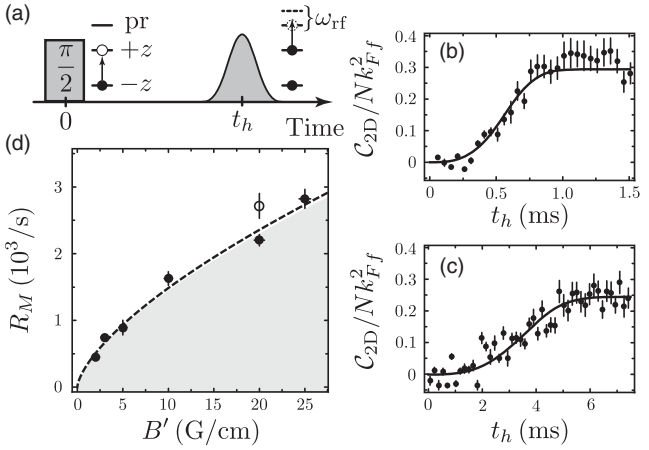

FIG. 4. Contact dynamics at $\ln(k_{Fi}a_{2D}) = 0.35(5)$ and $(T/T_F)_i = 0.31(2)$. (a) $\mathcal{C}_{2D}$ is measured after a hold time t_h by a pulse detuned by $\omega_{\rm rf}$ from the $|+z\rangle$-to-$|{\rm pr}\rangle$ transition. (b) Contact growth for $B' = 25$ G/cm. (c) Contact growth for $B' = 2$ G/cm. (d) The best-fit $R_M = (D_0^\perp \alpha^2)^{-1/3}$ determined from contact growth (black points) versus B'. The shaded region corresponds to R_M with $D_0^\perp < \hbar/m$. The open point indicates R_M from $\boldsymbol{M}$ dynamics at 20 G/cm. The dashed line shows the best-fit diffusivity $D_0^\perp = 1.1(1)\hbar/m$.

the trap explicitly breaks scale invariance, an SO(2,1) dynamical symmetry survives at the mean-field level [43] but is broken by a quantum anomaly whose expectation value is $\mathcal{C}_{2D}$ [21]. E is conserved in this isolated system; however, $\mathcal{C}_{2D}$ increases from zero for the noninteracting initial state to a finite positive value for the final state. This implies that V must also increase, which in turn dictates an increase in the rms cloud size: $V/N = \frac{1}{2}m(\omega_1^2\langle x_1^2\rangle + \omega_2^2\langle x_2^2\rangle)$.

Using rf spectroscopy, we measure $\mathcal{C}_{2D}$ throughout the demagnetization dynamics. The protocol is as described in Ref. [7] and depicted in Fig. 4(a). The dynamics are initiated with a $\theta = \pi/2$ pulse, and the sample is probed with a spectroscopic pulse that couples the states $|+z\rangle$ and $|{\rm pr}\rangle$ after a hold time t_h. The transfer rate of population to state $|{\rm pr}\rangle$ is measured as a function of the detuning $\omega_{\rm rf}$ from the bare spin-flip resonance and is known to scale with $\mathcal{C}_{2D}\omega_{\rm rf}^{-2}$ in the limit $\omega_{\rm rf} \gg E_F$ [34,44–46]. We compensate for final-state interactions between the $|{\rm pr}\rangle$ atoms and $|\pm z\rangle$ atoms in our analysis [28,34,47].

At $\ln(k_{Ff}a_{2D}) = 0.00(5)$, we find that the contact rises from zero to $\mathcal{C}_{2D}/N = 0.28(3)k_{Ff}^2$, where ${k_{Ff}}^2 = {k_{Fi}}^2/2$ after complete depolarization. Using Eq. (2), one finds $V - E/2 = 0.022(2)E_{Ff}$ per particle. In contrast, for a 3D gas at unitarity, the contribution of the contact to the virial is zero: $V - E/2$ is proportional to $\mathcal{C}_{3D}/a_{3D}$ and goes to zero when $a_{3D}^{-1} \to 0$.

A final thermodynamic transformation accompanying demagnetization is a temperature rise due to the combination of increased spin entropy and decreased occupation of the Fermi sea [48]. For an initial temperature of $0.3(1)T_{Fi}$ and a $\pi/2$ pulse, we observe $T_f = 0.7(2)T_{Ff}$ near $\ln(k_{Ff}a_{2D}) = 0$. Because of the released attractive interaction energy, this temperature rise is larger than the $T_f/T_{Ff} - T_i/T_{Fi} \approx 0.25$ one would expect from the demagnetization of an ideal gas. However, the temperature rise is 3 times smaller than the $T_f/T_{Ff} - T_i/T_{Fi} \approx 2.2$ that is predicted by matching the initial energy and number to the equilibrium 2D equation of state [49–51].

One interpretation of these observations is that few or no dimers are formed during demagnetization. This is certainly true when $a_{2D} < k_F^{-1}$, where the system is not a dimerized superfluid as it would be in the ground state. But even when $a_{2D} \sim k_F^{-1}$, measurements of T and $\mathcal{C}_{2D}$ suggest that the system remains in the *upper energetic branch*. The value of $\mathcal{C}_{2D}/Nk_F^2$ we observe is roughly 20 times smaller than the contact strength in an equilibrium mixture at $\ln(k_F a_{2D}) = 0$ [46,49]. The equilibrium contact is primarily due to a mean-field dimer contribution $\mathcal{C}_0 \approx 4Nk_F^2$. Without dimers, the contact in the upper branch would be due to short-range correlations of unbound atoms, and in fact the value we observe is comparable to $\mathcal{C}_{2D} - \mathcal{C}_0$ in the lower branch [52]. Unlike in 3D, the dimer binding energy in 2D is greater than E_F at the Feshbach resonance, so that an *attractive* upper branch is energetically well defined.

Figures 4(b) and 4(c) show the typical dynamics we observe when measuring $\mathcal{C}_{2D}(t_h)$. Because of Pauli exclusion, we can use such data to infer magnetization dynamics: Pairs of fermions must have a singlet wave function to interact through an s-wave contact interaction. The singlet fraction can be no larger than $1 - |\boldsymbol{M}|$ and would be $(1 - |\boldsymbol{M}|^2)/4$ for uncorrelated spins [7,53,54]. For the $\pi/2$ initialization pulse performed here, $|\boldsymbol{M}| = |M_{xy}|$, since $M_z = 0$. A direct comparison between $\boldsymbol{M}$ and $\mathcal{C}_{2D}$ at $B' = 20$ G/cm (see [28]) shows a correlation that lies between these two limits: $\mathcal{C}_{2D}/N$ is proportional to $1 - |M_{xy}(t_h)|^{1.4(2)}$. This form with $\gamma = 0.71$ is used to fit $\mathcal{C}_{2D}$ data for a variety of gradients [see Figs. 4(b) and 4(c)] and extract R_M.

Across the experimentally accessible gradients B', Fig. 4(d) shows a range of R_M from $4.4(2) \times 10^2$ to $2.9(2) \times 10^3$ s^{-1}. Throughout, R_M scales with $\alpha^{2/3}$ (see the dashed line) and can be explained by a single diffusivity $D_0^\perp = 1.1(1)\hbar/m$. This verifies that the microscopic $D_0^\perp$ is independent of B' across the accessible range and, thus, independent of the pitch of the spin helix. The comparable magnitude of $D_0^\perp$ determined by two measurement techniques is also a reassuring check on the fidelity of the spin-echo sequence used in $\boldsymbol{M}$ measurements, since the measurement of $\mathcal{C}_{2D}$ does not rely upon the successful rephasing of the spins at the echo time.

In summary, we observe quantum-limited spin transport in 2D Fermi gases when a_{2D} is tuned to be comparable to k_F^{-1}. We find that the conjectured lower bound $D_0^\perp \gtrsim \hbar/m$

is respected for all interaction strengths, temperatures, and applied field gradients accessible to our apparatus. This supports the generality of the bound $\tau_r^{-1} \lesssim k_B T/\hbar$ beyond quantum critical systems, since the finite $\mathcal{C}_{2D}$ observed in this system signifies a broken scaling symmetry near unitarity.

We thank A. Georges, A. Gezerlis, M. Köhl, S. Sachdev, E. Taylor, and Shizhong Zhang for stimulating discussions. This work is supported by the Natural Sciences and Engineering Research Council of Canada, by the Air Force Office of Scientific Research under FA9550-13-1-0063, and by the Army Research Office under W911NF-15-1-0603 and is part of and supported by the Deutsche Forschungsgemeinschaft Collaborative Research Centre "SFB 1225 (ISOQUANT)."

[1] P. K. Kovtun, D. T. Son, and A. O. Starinets, Phys. Rev. Lett. **94**, 111601 (2005); T. Schäfer and D. Teaney, Rep. Prog. Phys. **72**, 126001 (2009); A. Adams, L. D. Carr, T. Schäfer, P. Steinberg, and J. E. Thomas, New J. Phys. **14**, 115009 (2012).
[2] H. Song, Nucl. Phys. **A904–A905**, 114c (2013).
[3] C. Cao, E. Elliott, J. Joseph, H. Wu, J. Petricka, T. Schäfer, and J. E. Thomas, Science **331**, 58 (2011); E. Elliott, J. A. Joseph, and J. E. Thomas, Phys. Rev. Lett. **113**, 020406 (2014); J. A. Joseph, E. Elliott, and J. E. Thomas, Phys. Rev. Lett. **115**, 020401 (2015).
[4] T. Enss, R. Haussmann, and W. Zwerger, Ann. Phys. (Amsterdam) **326**, 770 (2011); T. Enss, Phys. Rev. A **86**, 013616 (2012).
[5] G. Wlazłowski, P. Magierski, and J. E. Drut, Phys. Rev. Lett. **109**, 020406 (2012); G. Wlazłowski, W. Quan, and A. Bulgac, Phys. Rev. A **92**, 063628 (2015).
[6] A. Sommer, M. Ku, G. Roati, and M. W. Zwierlein, Nature (London) **472**, 201 (2011); A. Sommer, M. Ku, and M. W. Zwierlein, New J. Phys. **13**, 055009 (2011); G. Valtolina, F. Scazza, A. Amico, A. Burchianti, A. Recati, T. Enss, M. Inguscio, M. Zaccanti, and G. Roati, arXiv:1605.07850.
[7] A. B. Bardon, S. Beattie, C. Luciuk, W. Cairncross, D. Fine, N. S. Cheng, G. J. A. Edge, E. Taylor, S. Zhang, S. Trotzky, and J. H. Thywissen, Science **344**, 722 (2014).
[8] S. Trotzky, S. Beattie, C. Luciuk, S. Smale, A. B. Bardon, T. Enss, E. Taylor, S. Zhang, and J. H. Thywissen, Phys. Rev. Lett. **114**, 015301 (2015).
[9] G. M. Bruun, New J. Phys. **13**, 035005 (2011); G. M. Bruun and C. J. Pethick, Phys. Rev. Lett. **107**, 255302 (2011).
[10] D. Wulin, H. Guo, C.-C. Chien, and K. Levin, Phys. Rev. A **83**, 061601 (2011); M. P. Mink, V. P. J. Jacobs, H. T. C. Stoof, R. A. Duine, M. Polini, and G. Vignale, Phys. Rev. A **86**, 063631 (2012); H. Heiselberg, Phys. Rev. Lett. **108**, 245303 (2012); H. Kim and D. A. Huse, Phys. Rev. A **86**, 053607 (2012); O. Goulko, F. Chevy, and C. Lobo, New J. Phys. **14**, 073036 (2012); T. Enss and R. Haussmann, Phys. Rev. Lett. **109**, 195303 (2012).
[11] T. Enss, Phys. Rev. A **88**, 033630 (2013).
[12] J. A. N. Bruin, H. Sakai, R. S. Perry, and A. P. Mackenzie, Science **339**, 804 (2013); J. C. Zhang, E. M. Levenson-Falk, B. J. Ramshaw, D. A. Bonn, R. Liang, W. N. Hardy, S. A. Hartnoll, and A. Kapitulnik, arXiv:1610.05845.
[13] S. A. Hartnoll, Nat. Phys. **11**, 54 (2015).
[14] S. Sachdev, *Quantum Phase Transitions* (Cambridge University Press, Cambridge, England, 1999).
[15] J. Zaanen, Nature (London) **430**, 512 (2004).
[16] P. Nikolic and S. Sachdev, Phys. Rev. A **75**, 033608 (2007).
[17] M. Y. Veillette, D. E. Sheehy, and L. Radzihovsky, Phys. Rev. A **75**, 043614 (2007).
[18] J. Hofmann, Phys. Rev. A **84**, 043603 (2011).
[19] G. M. Bruun, Phys. Rev. A **85**, 013636 (2012); T. Enss, C. Küppersbusch, and L. Fritz, Phys. Rev. A **86**, 013617 (2012).
[20] T. Schäfer, Phys. Rev. A **85**, 033623 (2012).
[21] J. Hofmann, Phys. Rev. Lett. **108**, 185303 (2012).
[22] E. Taylor and M. Randeria, Phys. Rev. Lett. **109**, 135301 (2012).
[23] J. Levinsen and M. Parish, Annu. Rev. Cold At. Mol. **3**, 1 (2015).
[24] M. Koschorreck, D. Pertot, E. Vogt, and M. Köhl, Nat. Phys. **9**, 405 (2013).
[25] E. Vogt, M. Feld, B. Fröhlich, D. Pertot, M. Koschorreck, and M. Köhl, Phys. Rev. Lett. **108**, 070404 (2012).
[26] A. J. Leggett and M. J. Rice, Phys. Rev. Lett. **20**, 586 (1968); A. J. Leggett, J. Phys. C **3**, 448 (1970).
[27] C. Chin, R. Grimm, P. Julienne, and E. Tiesinga, Rev. Mod. Phys. **82**, 1225 (2010).
[28] See Supplemental Material at http://link.aps.org/supplemental/10.1103/PhysRevLett.118.130405 for further details of the experimental and theoretical methods.
[29] E. L. Hahn, Phys. Rev. **80**, 580 (1950); H. Y. Carr and E. M. Purcell, Phys. Rev. **94**, 630 (1954); H. C. Torrey, Phys. Rev. **104**, 563 (1956).
[30] T. Enss, Phys. Rev. A **91**, 023614 (2015).
[31] J. R. Engelbrecht, M. Randeria, and L. Zhang, Phys. Rev. B **45**, 10135 (1992).
[32] D. S. Petrov and G. V. Shlyapnikov, Phys. Rev. A **64**, 012706 (2001).
[33] I. Bloch, J. Dalibard, and W. Zwerger, Rev. Mod. Phys. **80**, 885 (2008).
[34] C. Langmack, M. Barth, W. Zwerger, and E. Braaten, Phys. Rev. Lett. **108**, 060402 (2012).
[35] J. W. Jeon and W. J. Mullin, Phys. Rev. Lett. **62**, 2691 (1989).
[36] C. Lhuillier and F. Laloë, J. Phys. (Paris) **43**, 225 (1982).
[37] K. Miyake, W. J. Mullin, and P. C. E. Stamp, J. Phys. (Paris) **46**, 663 (1985).
[38] D. Pekker, M. Babadi, R. Sensarma, N. Zinner, L. Pollet, M. W. Zwierlein, and E. Demler, Phys. Rev. Lett. **106**, 050402 (2011); I. Sodemann, D. A. Pesin, and A. H. MacDonald, Phys. Rev. A **85**, 033628 (2012).
[39] S. Zhang and T.-L. Ho, New J. Phys. **13**, 055003 (2011).
[40] V. Pietilä, D. Pekker, Y. Nishida, and E. Demler, Phys. Rev. A **85**, 023621 (2012).
[41] F. Werner, Phys. Rev. A **78**, 025601 (2008); M. Valiente, N. T. Zinner, and K. Mølmer, Phys. Rev. A **84**, 063626 (2011).
[42] S. Tan, Ann. Phys. (Amsterdam) **323**, 2987 (2008); E. Braaten and L. Platter, Phys. Rev. Lett. **100**, 205301 (2008); S. Zhang and A. J. Leggett, Phys. Rev. A **79**, 023601

(2009); R. Combescot, F. Alzetto, and X. Leyronas, Phys. Rev. A **79**, 053640 (2009); F. Werner and Y. Castin, Phys. Rev. A **86**, 013626 (2012).
[43] L. P. Pitaevskii and A. Rosch, Phys. Rev. A **55**, R853 (1997).
[44] E. Braaten, D. Kang, and L. Platter, Phys. Rev. Lett. **104**, 223004 (2010).
[45] W. Schneider and M. Randeria, Phys. Rev. A **81**, 021601 (2010).
[46] B. Fröhlich, M. Feld, E. Vogt, M. Koschorreck, M. Kohl, C. Berthod, and T. Giamarchi, Phys. Rev. Lett. **109**, 130403 (2012).
[47] Y. Zhang, W. Ong, I. Arakelyan, and J. E. Thomas, Phys. Rev. Lett. **108**, 235302 (2012).
[48] R. Ragan, K. Grunwald, and C. Glenz, J. Low Temp. Phys. **126**, 163 (2002).
[49] G. Bertaina and S. Giorgini, Phys. Rev. Lett. **106**, 110403 (2011); M. Bauer, M. M. Parish, and T. Enss, Phys. Rev. Lett. **112**, 135302 (2014); H. Shi, S. Chiesa, and S. Zhang, Phys. Rev. A **92**, 033603 (2015); E. R. Anderson and J. E. Drut, Phys. Rev. Lett. **115**, 115301 (2015); A. Galea, H. Dawkins, S. Gandolfi, and A. Gezerlis, Phys. Rev. A **93**, 023602 (2016).
[50] K. Fenech, P. Dyke, T. Peppler, M. G. Lingham, S. Hoinka, H. Hu, and C. J. Vale, Phys. Rev. Lett. **116**, 045302 (2016).
[51] I. Boettcher, L. Bayha, D. Kedar, P. A. Murthy, M. Neidig, M. G. Ries, A. N. Wenz, G. Zürn, S. Jochim, and T. Enss, Phys. Rev. Lett. **116**, 045303 (2016).
[52] The peak "many-body contact" density in the lower branch is roughly $0.055k_F^4$ [49] and when divided by density $n = k_F^2/2\pi$ gives a bulk uniform contact $\mathcal{C}_{2D} - \mathcal{C}_0 \approx 0.35Nk_F^2$.
[53] G. S. Thekkadath, L. Jiang, and J. H. Thywissen, J. Phys. B **49**, 214002 (2016).
[54] W.-B. He, Y.-Y. Chen, S. Zhang, and X.-W. Guan, Phys. Rev. A **94**, 031604 (2016).